Low-temperature MIR to submillimeter mass absorption coefficient of interstellar dust analogues. II. Mg and Fe-rich amorphous silicates (Corrigendum)

K. Demyk, C. Meny, H. Leroux, C. Depecker, J. -B. Brubach, P. Roy, C. Nayral, W. -S. Ojo, F. Delpech

A&A 666, C4 (2022)
https://doi.org/10.1051/0004-6361/201730944e

Astronomy & Astrophysics

Low-temperature MIR to submillimeter mass absorption coefficient of interstellar dust analogues

II. Mg and Fe-rich amorphous silicates★

(Corrigendum)

K. Demyk [1], C. Meny[1], H. Leroux[2], C. Depecker[2], J.-B. Brubach[3], P. Roy[3], C. Nayral[4], W.-S. Ojo[4], and F. Delpech[4]

[1] IRAP, Université de Toulouse, CNRS, UPS, 9 avenue colonel Roche, BP 44346, 31028 Toulouse cedex 4, France
e-mail: karine.demyk@irap.omp.eu
[2] UMET, UMR 8207, Université Lille 1, CNRS, 59655 Villeneuve d'Ascq, France
[3] Ligne AILES – Synchrotron SOLEIL, L'Orme des Merisiers, 91192 Gif-sur-Yvette, France
[4] LPCNO, Université de Toulouse, CNRS, INSA, UPS, 135 avenue de Rangueil, 31077 Toulouse, France

A&A, 606, A50 (2017), https://doi.org/10.1051/0004-6361/201730944

Key words. dust, extinction – submillimeter: ISM – infrared: ISM – methods: laboratory: solid state – astrochemistry – errata, addenda

We would like to draw attention to the fact that the mass absorption coefficients (MACs) presented in the paper "Low-temperature MIR to submillimeter mass absorption coefficient of interstellar dust analogues. II. Mg and Fe-rich amorphous silicates" published in A&A 606, A50 (2017) are the MACs of the grains in the polyethylene matrix and not in vacuum. Indeed, Eq. (4) in Demyk et al. (2017) provides the MAC for the isolated grains in the matrix. The additional step to correct for the effect of the matrix, which is detailed in Mennella et al. (1998), was not done in Demyk et al. (2017). Therefore, in order to compare the experimental MACs presented in Demyk et al. (2017) with those calculated from optical constants available in databases or in cosmic dust models, it is necessary to perform the calculations in the same medium as that of the experimental data. This was not done in Demyk et al. (2017) in which Sect. 4.3, Table 2, Fig. 10, and Figs. A.1–A.8 compare MACs that are not comparable: the MAC for grains in polyethylene (PE) for the measurements and the MAC for grains in vacuum for the cosmic dust models. We provide here new versions of Table 2 and Figs. 10 and A.1–A.8 of Demyk et al. (2017) in which the MACs for the silicates from astronomical models are calculated in an ambient medium of refractive index n = 1.51 similar to that of the pellets (polyethylene). Table 1 and Fig. 1 of the corrigendum replace Table 2 and Fig. 10 of Demyk et al. (2017), respectively. Figures A.1–A.8 of the corrigendum replace Figs. A.1–A.8 of Demyk et al. (2017).

The main conclusions of the comparison of the experimental MAC with the MAC for cosmic dust models have not changed: in the 100 µm–1 mm range, the measured MAC is higher than that of cosmic models (see Table 1, Fig. 1, and Figs A.1–A.8). The factor of enhancement compared to the models depends on the sample and on the wavelength. It is in the range from 1 to 10 at 300 K and from 1 to 7 at 10 K, the highest factor being found at 500 and 850 µm. Considering the MAC averaged over all the samples, the value of $\langle \mathrm{MAC} \rangle_{\mathrm{all}}$ at 10 K is a little more than twice that of the modeled MAC in the range from 500 µm to 1 mm.

This also affects the comparison with previous experimental data if they are corrected for the effect of the matrix. Mennella et al. (1998) indicated that the matrix-correction factor is of the order of 1.3 for amorphous fayalite. Therefore, the MAC presented in Demyk et al. (2017) should be divided by a similar factor to be compared with experimental data from Mennella et al. (1998). However, for a more reliable comparison, we advise the use of the optical constants derived from these MACs by Demyk et al. (2022) to simulated the MAC of the grains in a vacuum.

★ Data from this article are publicly available through the STOPCODA (SpecTroscopy and Optical Properties of Cosmic Dust Analogues) database of the SSHADE infrastructure of solid spectroscopy (https://doi.org/10.26302/SSHADE/STOPCODA). The dataset are accessible via the following links: https://www.sshade.eu/data/experiment/EXPERIMENT_KD_20170822 and https://www.sshade.eu/data/experiment/EXPERIMENT_KD_20170823

References

Bohren, C. F., & Huffman, D. R. 1998, Absorption and Scattering of Light by Small Particles, eds. Bohren, C. F., & Huffman, D. R. (Hoboken: Wiley)
Demyk, K., Meny, C., Lu, X.-H., et al. 2017, A&A, 600, A123
Demyk, K., Gromov, V., Meny, C., et al. 2022, A&A, in press https://doi.org/10.1051/0004-6361/202243815
Jones, A. P., Fanciullo, L., Köhler, M., et al. 2013, A&A, 558, A62
Li, A., & Draine, B. T. 2001, ApJ, 554, 778
Mennella, V., Brucato, J. R., Colangeli, L., et al. 1998, ApJ, 496, 1058

Table 1. Value of the MAC of the E10, E20, E30, E40, E10R, E20R, E30R, and E40R samples in the polyethylene matrix compared with that of the silicate component of cosmic dust models in polyethylene.

	Mass absorption coefficient in polyethylene ($cm^2\ g^{-1}$)									
	100 μm		250 μm		500 μm		850 μm		1 mm	
	10 K	300 K	10 K	300 K	10 K	300 K	10 K	300 K	10 K	300 K
E10	260.0	305.3	37.7	92.6	7.2	20.6	1.0	6.0	–	–
E20	224.8	243.5	46.2	58.8	6.8	14.2	1.5	4.9	1.0	3.7
E30	195.2	217.8	41.0	52.9	7.6	14.1	2.8	6.0	2.4	5.1
E40	219.3	245.0	35.7	62.5	5.8	15.7	2.2	7.0	2.0	6.1
E10R	244.0	270.4	57.5	80.0	11.5	23.6	3.9	10.4	3.5	8.9
E20R	249.4	268.6	55.1	79.2	14.4	24.6	7.0	12.2	5.8	10.1
E30R	225.7	253.9	44.7	67.3	6.8	18.8	1.4	8.0	0.8	6.2
E40R	195.2	219.0	39.2	53.7	5.0	15.2	1.3	7.4	1.0	6.1
$\langle MAC \rangle_{Exx}$ [(1)]	225	253	40	67	6.8	16.1	1.9	6.0	1.4	4.8
$\langle MAC \rangle_{ExxR}$ [(2)]	229	253	49	70	9.4	20.6	3.4	9.5	2.8	7.8
$\langle MAC \rangle_{all}$ [(3)]	227	253	45	68	8.1	18.3	2.6	7.7	2.1	6.3
MAC sphere 0.1 μm [(3)]	82		12.6		2.8		1.15		0.9	
MAC distrib spherical grains [(3)]	84.2		12.6		2.8		1.15		0.9	
MAC CDE [(4)]	74.0		11.5		2.6		1.05		0.81	

Notes. See Sects. 4.1 and 4.3 of Demyk et al. (2017). [(1)]MAC averaged over the four unprocessed samples E10, E20, E30, and E40. [(2)]MAC averaged over the four processed samples E10R, E20R, E30R, and E40R. [(3)]MAC averaged over the eight samples E10, E20, E30, E40 and E10R, E20R, E30R, and E40R. [(4)]These MACs were calculated in an ambient medium of refractive index $n = 1.51$ (corresponding to PE) and using the optical constants of the "astrosilicates" from Li & Draine (2001).

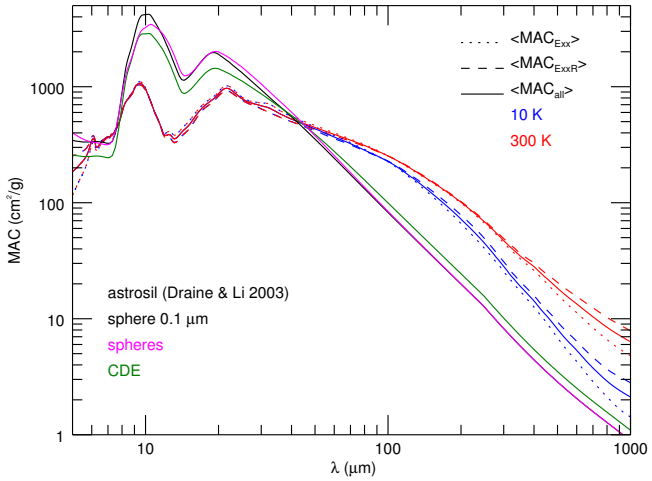

Fig. 1. Comparison of the average MAC at 10 and 300 K with astronomical dust models. The MAC of the "astrosilicates" from Li & Draine (2001) were calculated using Mie theory for a 0.1 μm size grain (black), for a log-normal grain-size distribution with a mean diameter of 1 μm for spherical grains (magenta), and for a continuous distribution of ellipsoids (CDE, green). We note that to be comparable with the experimental data, the MAC are modelled in PE and not in vacuum.

Appendix A: Comparison with astronomical models

Figures A.1 to A.8 show the comparison of the MAC for each sample with the MAC calculated for the *astrosil* model (Li & Draine 2001) and for the THEMIS model (Jones et al. 2013). The calculations were performed using Mie theory (Bohren & Huffman 1998) for a spherical particle with a size of 100 nm, for spherical grain populations with a log-normal size distribution centered at 1 µm, and for a CDE distribution (green). We note that to be comparable with the experimental data, the MAC are modelled in PE and not in vacuum.

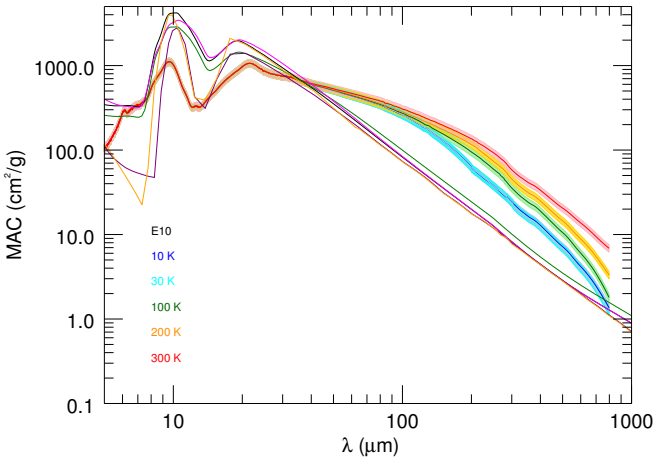

Fig. A.1. Comparison of the MAC of sample E10 with the MAC calculated for astronomical dust models. The MAC calculated with the *astrosil* is shown for a 0.1 µm size grain (black), for a log-normal grain size distribution with a mean diameter of 1 µm for spherical grains (magenta), and for a CDE distribution (green). The MAC calculated with the THEMIS dust model is shown for a spherical grain of 100 nm in diameter for amorphous forsterite (purple) and amorphous enstatite (orange).

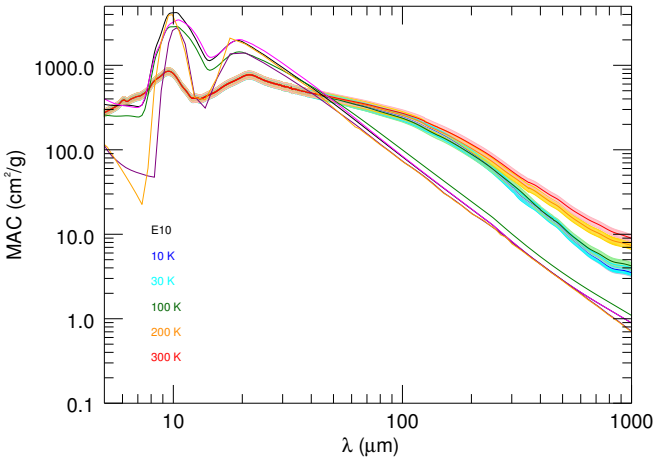

Fig. A.2. Comparison of the MAC of sample E10R with the MAC calculated for astronomical dust models. The MAC calculated with the *astrosil* is shown for a 0.1 µm size grain (black), for a log-normal grain size distribution with a mean diameter of 1 µm for spherical grains (magenta), and for a CDE distribution (green). The MAC calculated with the THEMIS dust model is shown for a spherical grain of 100 nm in diameter for amorphous forsterite (purple) and amorphous enstatite (orange).

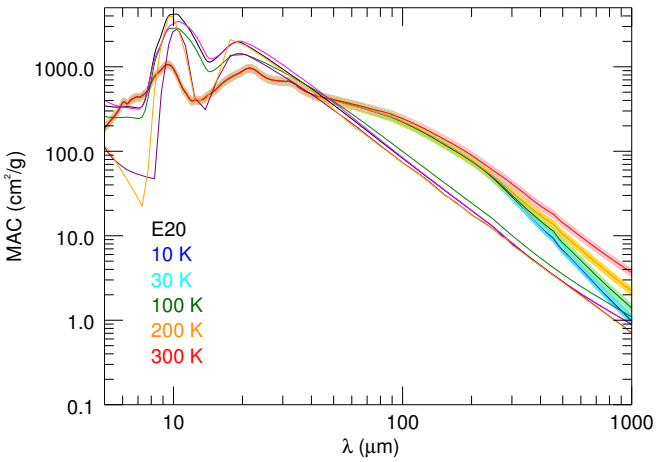

Fig. A.3. Comparison of the MAC of sample E20 with the MAC calculated for astronomical dust models. The MAC calculated with the *astrosil* is shown for a 0.1 µm size grain (black), for a log-normal grain size distribution with a mean diameter of 1 µm for spherical grains (magenta), and for a CDE distribution (green). The MAC calculated with the THEMIS dust model is shown for a spherical grain of 100 nm in diameter for amorphous forsterite (purple) and amorphous enstatite (orange).

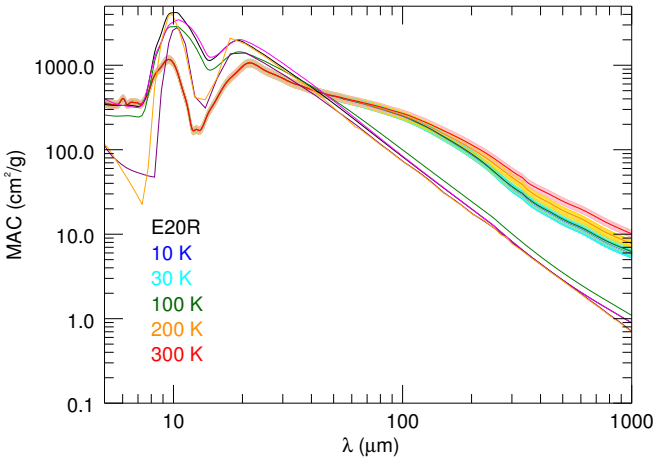

Fig. A.4. Comparison of the MAC of sample E20R with the MAC calculated for astronomical dust models. The MAC calculated with the *astrosil* is shown for a 0.1 µm size grain (black), for a log-normal grain size distribution with a mean diameter of 1 µm for spherical grains (magenta), and for a CDE distribution (green). The MAC calculated with the THEMIS dust model is shown for a spherical grain of 100 nm in diameter for amorphous forsterite (purple) and amorphous enstatite (orange).

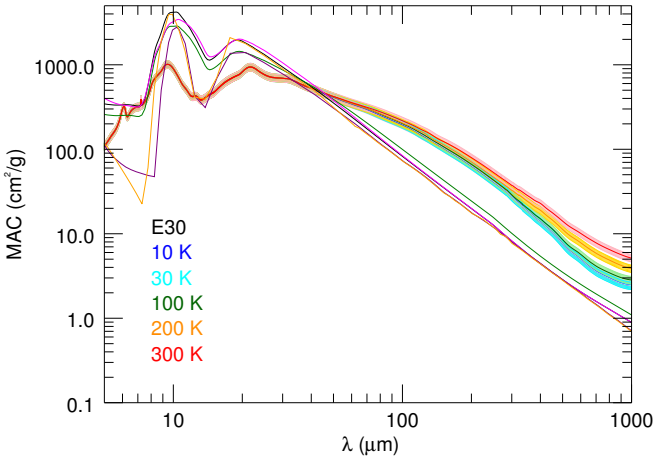

Fig. A.5. Comparison of the MAC of sample E30 with the MAC calculated for astronomical dust models. The MAC calculated with the *astrosil* is shown for a 0.1 μm size grain (black), for a log-normal grain size distribution with a mean diameter of 1 μm for spherical grains (magenta), and for a CDE distribution (green). The MAC calculated with the THEMIS dust model is shown for a spherical grain of 100 nm in diameter for amorphous forsterite (purple) and amorphous enstatite (orange).

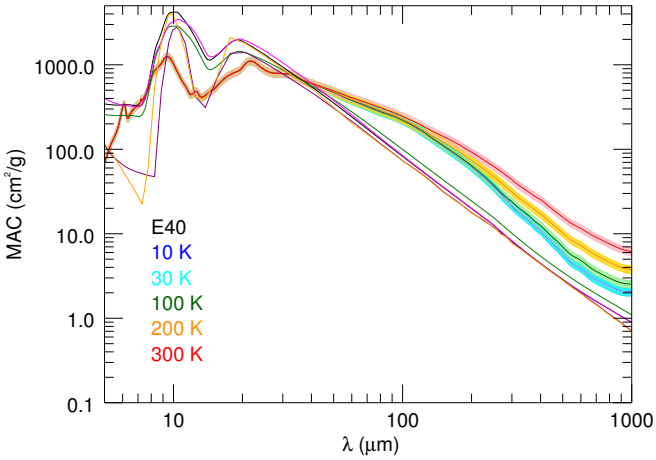

Fig. A.7. Comparison of the MAC of sample E40 with the MAC calculated for astronomical dust models. The MAC calculated with the *astrosil* is shown for a 0.1 μm size grain (black), for a log-normal grain size distribution with a mean diameter of 1 μm for spherical grains (magenta), and for a CDE distribution (green). The MAC calculated with the THEMIS dust model is shown for a spherical grain of 100 nm in diameter for amorphous forsterite (purple) and amorphous enstatite (orange).

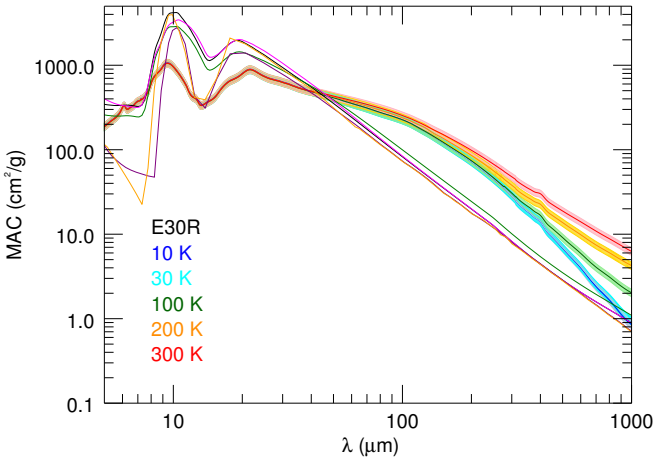

Fig. A.6. Comparison of the MAC of sample E30R with the MAC calculated for astronomical dust models. The MAC calculated with the *astrosil* is shown for a 0.1 μm size grain (black), for a log-normal grain size distribution with a mean diameter of 1 μm for spherical grains (magenta), and for a CDE distribution (green). The MAC calculated with the THEMIS dust model is shown for a spherical grain of 100 nm in diameter for amorphous forsterite (purple) and amorphous enstatite (orange).

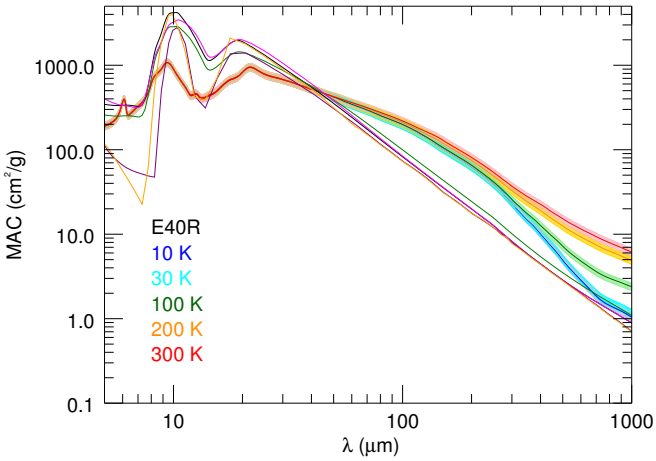

Fig. A.8. Comparison of the MAC of sample E40R with the MAC calculated for astronomical dust models. The MAC calculated with the *astrosil* is shown for a 0.1 μm size grain (black), for a log-normal grain size distribution with a mean diameter of 1 μm for spherical grains (magenta), and for a CDE distribution (green). The MAC calculated with the THEMIS dust model is shown for a spherical grain of 100 nm in diameter for amorphous forsterite (purple) and amorphous enstatite (orange).